High-temperature PEM Fuel Cell Characterization: an Experimental Study Focused on Potential Degradation due to the Polarization Curve

Mathieu Baudy[1,*], *Amine* Jaafar[1], *Christophe* Turpin[1], *Sofyane* Abbou[2] and *Sylvain* Rigal[1]

[1]LAPLACE, Université de Toulouse, CNRS, INPT, UPS, Toulouse, France
[2]Safran Power Units, F-31019 Toulouse, France

Abstract. High-Temperature Proton Exchange Membrane Fuel Cell constant current ageing tests highlighted that the characterizations used to monitor the state of health of single cells could be potentially degrading. An experimental campaign to analyze potential degradation due to polarization curves was carried out. More exactly, four methodologies to generate a polarization curve including Electrochemical Impedance Spectroscopies (EIS) were cycled 30 times. The tested single cells were based on a commercial PBI Membrane Electrodes Assembly (MEA) with an active surface of 45 cm² (BASF Celtec®-P 1100 type). Before the first cycling test and after the last cycling one, complete characterizations, composed by a voltammetry and a polarization curve including EIS, were performed. The results show that one of the MEA has a voltage which increased for one of the four methods to obtain the polarization curve. This growth is linked to a decrease of ohmic losses: in an unexpected way, it could be considered as a way to improve the break-in period. Similarly, the monitoring of CO_2 emission (as corrosion has been suspected to be involved at high voltage, i.e. low current density) confirms the potential degradation of the electrodes during the measurement of the polarization curve.

1 Introduction

1.1 Study context

The use of fuel cells for aeronautical applications is proposed as one of the technological solutions, in order to decarbonize this sector responsible for 2-6 % of the global radiative forcing [1]. In 2018, 11 % of the world's population flew at least once, while only 1 % emits 50 % of CO_2 from commercial aviation [2]. In this context, aircraft manufacturers are predicting a doubling of the global fleet by 2035 [3,4]. The scenarios envisaged in order to achieve the decarbonization objectives set by the European Commission, propose using fuel cells to power electric engines of light (<80 passengers), short and medium-haul (<1000 km) aircrafts [5]. This use should reduce the impact on the climate of this market segment by 75 to 90 % [5].

As part of the PIPAA ("PIle à combustible Pour Applications Aéronautiques") project led by Safran Power Units, a fuel cell system is to be developed to supply a number of secondary loads on a business aircraft [6]. These may be, for example, galley equipment, entertainment equipment or auxiliary power units [7]. For these uses, the main characteristics expected from a power generation system are to be as compact and light as possible.

Developed in the 1990s, the HT-PEMFC (High Temperature Proton Exchange Membrane Fuel Cell) operates between 120 and 200 °C thanks to a PoliBenzImidazole (PBI) polymer membrane doped with phosphoric acid (H_3PO_4). The HT-PEMFC provides several advantages compared to the LT-PEMFC (Low Temperature Proton Exchange Membrane Fuel Cell): (i) a better tolerance to carbon monoxide CO [8-10], which allows it, for example, a facilitated use with H_2 coming directly from the steam-reforming of hydrocarbide (95 % of the current world production) or biomethane, (ii) a use with dry gases [10,11] (it is not necessary to use a gas humidification system), (iii) a simplified thermal management (an easier cooling at higher ambient temperatures that could be a real advantage for transport applications with very high ambient temperature as an aircraft on the tarmac of an airport in an arid zone). Its main disadvantages compared to the LT-PEMFC are: (i) its longer start-up time (the fuel cell must be preheated to avoid the presence of liquid water harmful to the electrolyte) [9], (ii) accelerated degradative side reactions (catalyzed by the higher temperature) [9], (iii) decreased kinetics of the oxygen reduction reaction (by adsorption of H_3PO_4 on the platinum catalyst of the electrode) [12-14]. Despite these drawbacks, the HT-PEMFC advantages make it an interesting candidate to meet the different expectations.

* Corresponding author: baudy@laplace.univ-tlse.fr

1.2 Study issues

Since 2015, several research works at the LAPLACE laboratory have been focused on the HT-PEMFC study. In particular, the work done by S. Rigal et al [15,16] has validated the use of a semi-empirical model, for the analysis of quasi-static performance, as a function of the operating conditions. The model was developed from a design of experiment carried out by varying the current, the temperature and the stoichiometry of the reactive gases. This work allowed mapping the operating ranges of different HT-PEMFC Membrane-Electrode Assembly (MEA) technologies, in order to compare their performances. In addition, ageing tests at different constant currents for about 540 hours (see Fig. 1) were performed on commercial MEAs of the BASF Celtec®-P 1100 type (manufactured by the Advent company). In order to monitor the health of the MEAs, several experimental characterizations were performed: (i) polarization curves, named *v*(*i*) (to describe the quasi-static state, representing the evolution of the voltage as a function of the current density), (ii) Electrochemical Impedance Spectroscopies named EIS (to describe the dynamic state, by representing the response of the system to a sinusoidal solicitation of low amplitude in current, between 20 kHz and 1 Hz around an operating point), (iii) sinusoidal scans in current of high amplitude at low frequency, (iv) cyclic voltammetries (potentiostatic scans in H_2/N_2). The ageing rates calculated from the fuel cell voltage, over the duration of the tests and for the different MEAs, are five times greater than those commonly found in the literature (e.g., -25 µV.h^{-1} at 0.2 A.cm^{-2} instead of -5 µV.h^{-1} [10,17-20]). Also, following the characterization phases, voltage drops have been observed (see Fig. 1).

In the work of S. Rigal et al [16], a first degradation path is proposed as being the corrosion of carbon. It occurs usually at high voltages (>0.8 V) in presence of water [21]. These high voltages are explored during the various characterizations and particularly at Open Circuit Voltage (OCV). A complementary aging test of 540 h on a new MEA with truncated *v*(*i*) (i.e. the high voltages are explored by limiting the current density to 0.2 A.cm^{-2}, noted MEA0.2* in Fig. 1) has been performed. The observed effect is particularly important at high current densities: 30 % less voltage degradation, calculated from the polarization curves at 1.1 A.cm^{-2} (about +23 mV). In addition, an aging test with a new MEA under the same conditions (160 °C, H_2/AIR at 1.2/2 stoichiometry and without pressure regulation) was also performed. This test lasted 2400 h at four successive current densities (0.2, 0.4, 0.6 and 0.2 A.cm^{-2}) every 600 h and without any follow-up characterizations. Only reference characterizations truncated at 0.2 A.cm^{-2} were performed, at the beginning and at the end of the test. Ageing rates close to those reported in the literature were obtained for the different tested currents. Thus, the main hypothesis for the origin of the observed degradations, is related to the characterizations. Consequently, it was decided to verify and quantify the potential degrading character of one of the characterizations carried out during the ageing tests: the polarization curve.

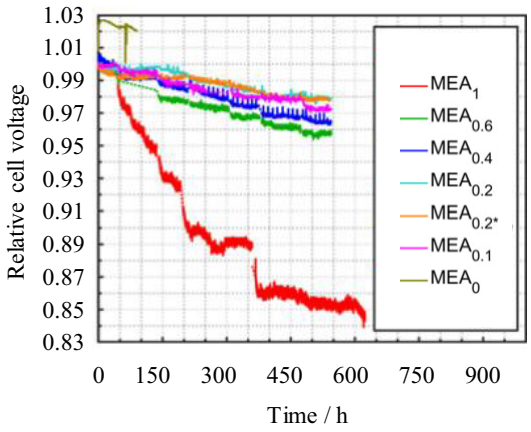

Fig. 1. Voltages referred to the initial voltage of 7 MEAs aging at different constant currents (from 0.1 to 1 A.cm^{-2}, at 160 °C, in H_2/AIR at stoichiometries of 1.2/2 and without pressure regulation). The characterizations have been replaced by dotted lines for better lisibility. Figure from [16].

Several methodologies for realizing the polarization curve have been identified in the literature. Two projects, funded by the Fuel Cells and Hydrogen Joint Undertaking (FCH-JU), named respectively CISTEM (Construction of Improved HT-PEM MEAs and Stacks for Long Term Stable Modular CHP Units, 2013-2016) and DEMMEA (Understanding the Degradation Mechanisms of Membrane-Electrode-Assembly for High Temperature PEMFCs and Optimization of the Individual Components, 2010-2012) were specifically interested in the HT-PEMFC technology and more particularly in the implementation of standardized operating procedures to carry out characterizations. The procedure concerning the polarization curve is inspired by an old version of the AFNOR 62282-7-1 standard which has been adapted for the HT-PEMFC. This procedure has been included, in a specific chapter on characterization, in the 2016 reference book on HT-PEMFC from the publisher Springer [21].

The proposed methodologies mainly ensure the quasi-static character of the polarization curve. Following the first observations made previously, different phenomena specific to the HT-PEMFC must also be taken into account when choosing a methodology for the realization of the polarization curve. It must, for example, be the least intrusive possible. For that, it must avoid degrading the fuel cell. Therefore, it is important to know the degradation mechanisms that the polarization curve is likely to solicit and to avoid or minimize them. For example, in the case of carbon corrosion, which often occurs at high voltages, truncating the polarization curve in current can be justified to avoid degradation. The use of discharge resistors can then avoid the HT-PEMFC to explore these high voltages, as it was already done for PAFCs.

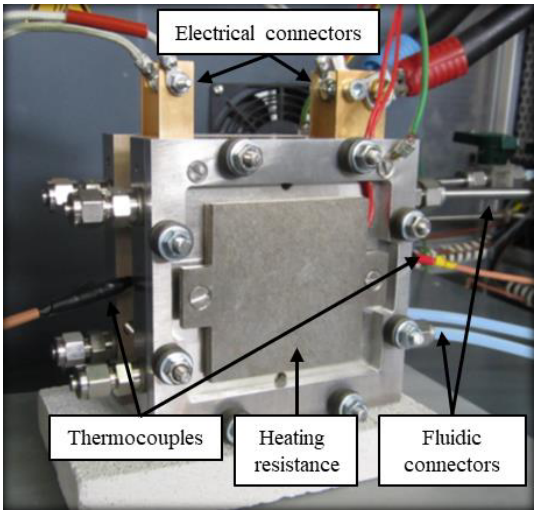

Fig. 2. Photo of the BASF HT-PEMFC single-cell fuel cell installed in the Laplace lab test bench.

2 Experimental tests

2.1 Test specimen and test bench

Commercial MEAs of the BASF Celtec®-P 1100 type (manufactured by Advent) with an active surface area of 45.2 cm^2 are used to perform these tests. They are installed in a single-cell box, manufactured by BASF (see Fig. 2). This box is made of graphite gas flow plates, copper current collector plates and clamping end plates including the distribution and extraction of the fuel cell gases.

The single cell box is installed in an in-house test bench that can operate with H_2, air and N_2 gases. It includes fluidic equipment to distribute and extract these gases and to carry out the flow regulation. It also has electrical equipment to regulate the fuel cell current and the fuel cell temperature. An atmospheric pressure sensor is installed in the test bench since the fuel cell anodic and cathodic compartments are not regulated. It should be noted that the exhaust pipes are immersed in water pots in order to purify the gases before rejecting them to the atmosphere. This system generates very little pressure drop and consequently the anode and the cathode outlet pressures are very close to atmospheric pressure.

2.2 Initial phase and baseline characterizations

For the test campaign performed during this study, particular attention is given to the development of operating procedures for the test initial phase. The aim is to limit the degradation during this step. The test initial phase is composed of different parts: (i) the assembly of the MEA in the box, (ii) the box installation in the test bench, (iii) the temperature rise followed by the fuel cell start-up, (iv) the break-in (specific early life operation to improve reproducibility and performance), (v) an initial characterization phase. The main changes, compared to the operating procedures of the previously presented campaigns [15,16], consisted in: (i) limiting the generation of local high potentials (during gas changes occurring for start-ups and voltammetries) by using a discharge resistor connected to both MEA electrodes during transient phases when the fuel cell current is not regulated, (ii) perform active gases at 120 °C to limit the degradation linked to secondary reactions (catalyzed by the high temperature), (iii) use the break-in procedure specifically proposed by the MEA manufacturer (14 h at 0.2 $A.cm^{-2}$ and 180 °C). Following the fuel cell break-in, a cyclic voltammetry (in H_2/N_2 at 0.2 $NL.min^{-1}$, from 30 mV to 800 mV and at a speed of 40 $mV.s^{-1}$) is performed, followed by an initial reference $v(i)$ (identical for each cycle). The characterization phase including the cyclic voltammetry and the $v(i)$ is performed at the end of the test. The aim is to make a comparison of the collected data, by carrying out the same procedure whatever the test.

2.3 Cycling test

Four MEAs are used to cycle four different current profiles 30 times (see Fig. 3). Each current profile allows to perform a polarization curve (four polarization curves are obtained in total) and then finishes with a stabilization phase (see Fig. 4). This phase takes place at constant current. Its duration is determined so that the cycle lasts 70 h in total (see Fig. 3 and Table 1). It is therefore different for each cycle. All the tests are carried out at 160 °C, in H_2/AIR at respective stoichiometries 1.2/2 and without pressure regulation. Each cycle will be named $v(i)\_j$ where j represents the number of the MEA used (between 1 and 4 inclusive). The MEA will also be identified by MEA j. The number of repetitions of the current profile related to each $v(i)$ has been chosen by taking into account the perspective of performing aging tests of 3000 h. Indeed, by monitoring the MEA health every 100 h, 30 $v(i)$ will be performed. Thus, it seems interesting to study the impact of these $v(i)$ on the ageing tests. To perform a $v(i)$, each current profile starts from the first indicated current density value and finishes with the final current density, shown in Table 1. Several current ramps are therefore performed to reach the levels where a stabilization and voltage reading are performed. The ramps and stabilizations are defined to achieve stable operating conditions for the $v(i)$ steps. Current ramps are also performed, to reach and return to the stabilization phase current.

The cycles can be differentiated by several characteristics: (i) the direction of the imposed current profile ($v(i)\_1$ and $v(i)\_2$ perform the current profile in an increasing way and inversely for the cycles $v(i)\_3$ and $v(i)\_4$, cf. Fig. 4), (ii) the passage or not to 0 $A.cm^{-2}$ (only $v(i)\_3$ performs OCV measurements), (iii) the passage to the low current densities lower than 0.2 $A.cm^{-2}$ ($v(i)\_4$ is truncated in current), (iv) the passage to a current density of 1.1 $A.cm^{-2}$ ($v(i)\_3$ and $v(i)\_4$ stabilize at 1.1 $A.cm^{-2}$ after the current ramp performed between the stabilization point and the starting point of $v(i)$), (v) the stabilization current density ($v(i)\_2$ has exactly the same current profile as $v(i)\_1$ but stabilizes at 0.6 $A.cm^{-2}$). Note that it is the $v(i)\_1$ current profile (see Fig. 4) that is used

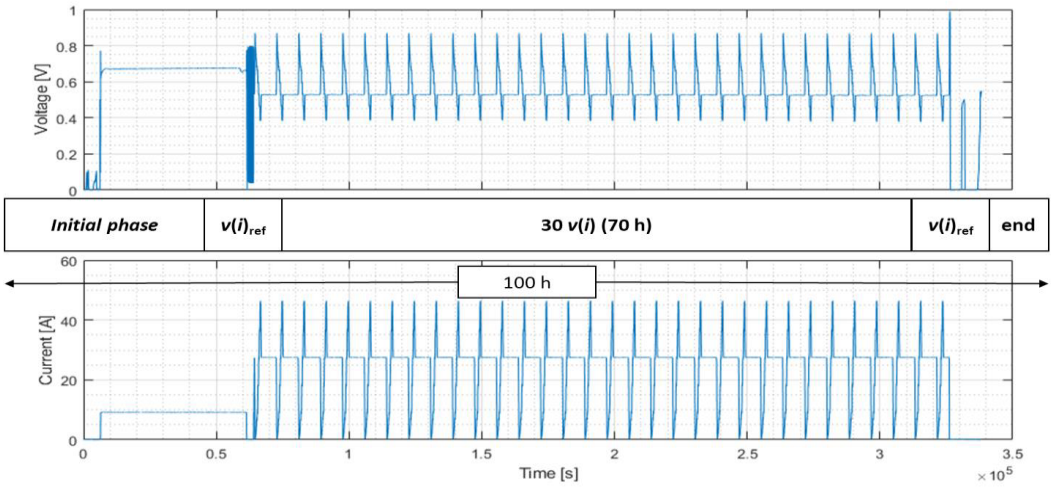

Fig. 3. *v*(*i*)_2 cycle current profile and fuel cell voltage response.

Table 1. Definition of the four performed cycles.

Cycle	Current profile and duration of the *v*(*i*)	Current density and duration of the stabilization.
v(*i*)_1	0.004 to 1 A.cm^{-2} (40 min)	0.2 A.cm^{-2} (95 min)
v(*i*)_2	0.004 to 1 A.cm^{-2} (40 min)	0.6 A.cm^{-2} (95 min)
v(*i*)_3	1.1 to 0 A.cm^{-2} (82 min)	0.2 A.cm^{-2} (53 min)
v(*i*)_4	1.1 to 0.2 A.cm^{-2} (58 min)	0.2 A.cm^{-2} (87 min)

to make the initial and final reference polarization curves. In addition, EIS (from 20 kHZ to 1 Hz) are performed during some steps of the polarization curves (not shown in Fig. 4). The EIS is used to measure the high frequency resistance (R_{HF}). This resistance is taken at the frequency where the fuel cell impedance spectrum is composed of only a real part.

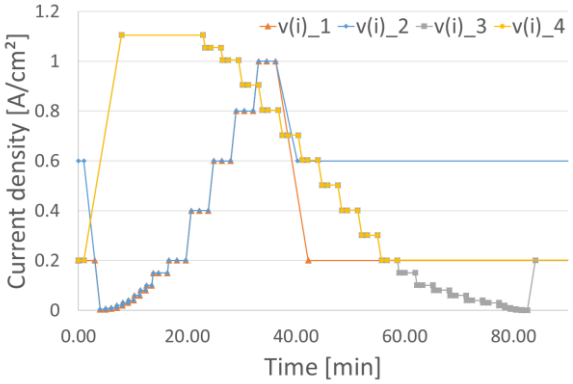

Fig. 4. Current profiles used for the four cycles.

3 Results

3.1 Reproducibility of the initial test phase

We observe, in Fig. 5, the increase of the voltage, during the break-in period. This increase is similar for the four MEAs. It should be noted that the atmospheric pressure has an impact on the voltage, by its direct effect on the partial pressures of the gases within the electrodes. At constant flow rate, an increase of the atmospheric pressure will lead to an increase of the voltage. Moreover, at constant atmospheric pressure, the increase in flow will also generate greater pressure drops.

The implementation of the operating procedures at the beginning of the tests allows a good reproducibility between each MEA, following the initial reference *v*(*i*) (cf. Fig. 6). Indeed, the maximum deviation from the mean value is obtained at 1 A.cm^{-2}. It is equal to 7 mV, i.e. 1.86 % relative to the mean voltage (with a standard deviation of 5.5 mV). It can be noted that it is the MEA 4, which does not come from the same batch, which increases this deviation (1 mV of maximum deviation from the mean without MEA 4).

3.2 Comparison of initial and final reference *v*(*i*)

To compare the different cycles, the voltages recorded for each current of the steps of the reference polarization curves are subtracted. Also, a particular interest is given to the results at 1 A.cm^{-2} where the voltage differences are the most important (see Table 2). The aging rates μ are calculated from the voltages at 1 A.cm^{-2} of the initial $U_{init}(i)$ and final $U_{final}(i)$ reference polarization curves, with a test duration of Δt=70 h in accordance with equation 1. The atmospheric pressures P_{atm}, at the time of the voltages reading, are given as an indication.

$$\mu=[U_{final}(1\ \text{A.cm}^{-2})-U_{init}(1\ \text{A.cm}^{-2})]\ \Delta t^{-1} \quad (1)$$

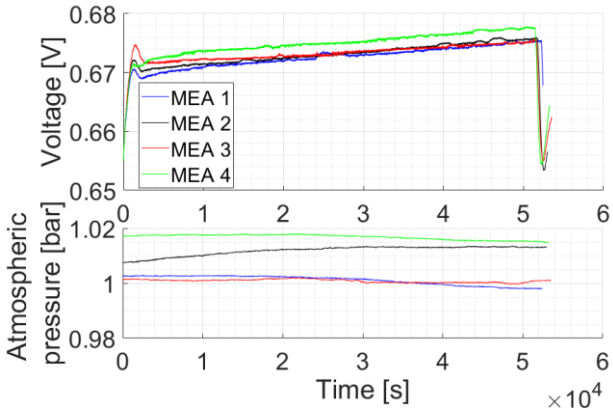

Fig. 5. Voltage and atmospheric pressure during the break-in period of the four MEAs at 180 °C, at 9 A or 0.2 A.cm^{-2} during 14 h.

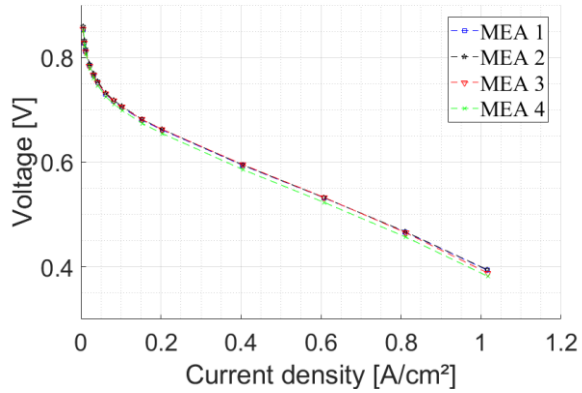

Fig. 6. Initial reference polarization curves of the 4 MEAs (cycle current profile *v*(*i*)_1, 160 °C, in H_2/AIR at 1.2/2 stoichiometries). Atmospheric pressures are given as an indication.

3.3 Evolution of the *v*(*i*) regarding each cycles

As can be observed in Fig. 7, the disparities are relatively small between the different sets composed by the *v*(*i*) of each cycle. It is interesting to note that the obtained voltages on the polarization curves *v*(*i*)_1 and *v*(*i*)_2 cycles (where the *v*(*i*) are realized by current increase) are slightly better at high current densities. Also, the *v*(*i*) voltages of the *v*(*i*)_3 and *v*(*i*)_4 cycles are slightly better at low current densities.

3.4 Evolution of the stabilization phases

Analysis of the stabilization phases (see Fig. 8) shows similar changes in relative voltages for the *v*(*i*)_1 and *v*(*i*)_3 cycles. The cycle *v*(*i*)_4 has a voltage that decreases slightly before stabilizing. Finally, the *v*(*i*)_2 cycle has a decreasing relative voltage. Note that the voltages were related to the voltage measured at the end of the first stabilization phase, after the initial reference polarization curve. Indeed, since the *v*(*i*)_2 cycle performs its stabilization at a higher current density (0.6 A.cm^{-2}), this allows us to compare the evolution of the four cycles along the time.

Table 2. Voltages measured at 1 A.cm^{-2} and ageing rate.

	***v*(*i*)_1**	***v*(*i*)_2**	***v*(*i*)_3**	***v*(*i*)_4**
U_{init} (1 A.cm^{-2}) [mV]	393	394	388	381
P_{atm} [barA]	0.997	1.012	1.001	1.014
U_{final} (1 A.cm^{-2}) [mV]	401	390	388	387
P_{atm} [barA]	1.007	0.982	1.009	1.002
μ [µV.h^{-1}]	114	-57	0	85

The voltage of cycles *v*(*i*)_1 and *v*(*i*)_4 have increased, cycle *v*(*i*)_3 remained globally neutral and cycle *v*(*i*)_4 lost voltage. Fig. 9 shows the evolution of atmospheric pressure along the time. It is interesting to note that the evolution of the relative voltages, seems similar to that of the atmospheric pressures.

4 Results analysis and discussion

4.1 Comparison of cycles

The results, from the comparison of the initial and final reference *v*(*i*), allow distinguishing two cycles that improve the voltage (*v*(*i*)_1 and *v*(*i*)_4) and two others that slightly degrade it (v(i)_2 and *v*(*i*)_3). The only difference between *v*(*i*)_1 and *v*(*i*)_2 is the stabilization current. Also, the stabilization current of *v*(*i*)_2 at 0.6 A.cm^{-2} seems to have been degrading for the voltage. However, this result must be nuanced. Indeed, the impact of the variation of the atmospheric pressure can have a significant effect on the voltage. Particularly, if we analyze the atmospheric pressures in Table 2, which can also be seen in Fig. 9, the final reference polarization curve of the *v*(*i*)_2 cycle is performed at a low atmospheric pressure.

Comparing the references of the v(*i*)_4 cycle (characterized by a current-truncated v(*i*)) with the other cycles, it can be seen that it does not necessarily seem more degrading to explore high voltages. If we observe the evolution of the *v*(*i*) voltages for the *v*(*i*)_4 cycle, we can see that they decrease during the test. Nevertheless, by comparing the reference polarisation curves, a voltage improvement is noted. It is indeed the final reference *v*(*i*) that has a beneficial effect on the voltages. This suggests that the repetition of the *v*(*i*)_4 cycle current profile results in an accumulation of reversible losses. This idea is reinforced by the fact that *v*(*i*)_1 also increased in performance during each *v*(*i*) cycle (as a reminder, this is the current profile used for the reference polarization curves). In addition, the *v*(*i*)_3 cycle had no overall effect

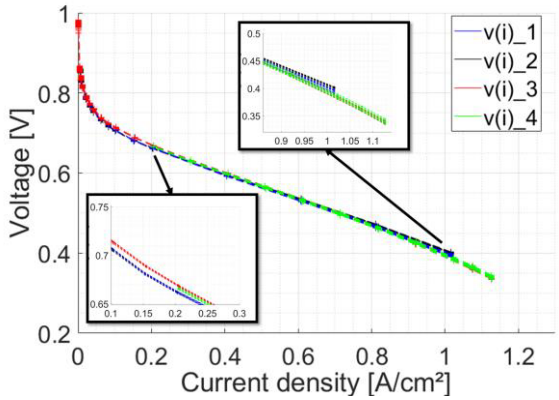

Fig. 7. All 30 polarization curves performed for each cycle (reference polarization curves are not plotted).

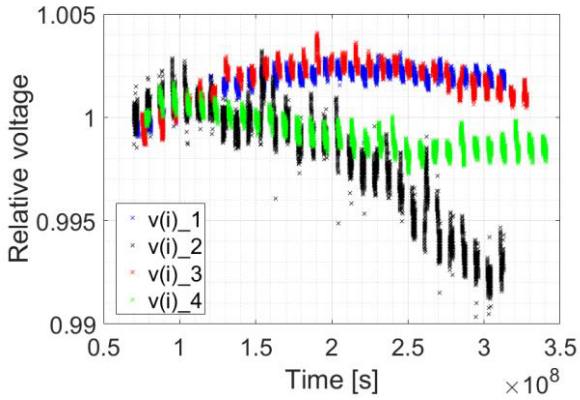

Fig. 8. Voltage evolution of the stabilization phases of the four cycles. The $v(i)$ have been removed to improve readability.

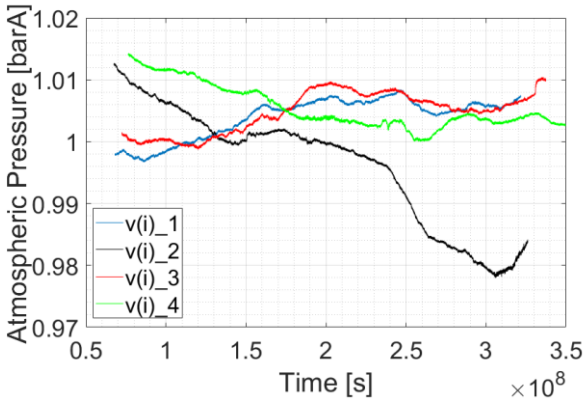

Fig. 9. Variation of the atmospheric pressure during the different cycles. A similar evolution of pressure and voltage is observed, particularly visible for the cycle $v(i)$_2.

on the voltages. This was the only current profile that measures open circuit voltage. As with the $v(i)$_4 cycle, the $v(i)$ started at high currents (1.1 A.cm^{-2}). It thus seems that the switch to low current densities did have a negative effect. This is the hypothesis that had already been considered by Rigal et al [15,16]. Moreover, if we establish that the final reference $v(i)$ eliminates the reversible losses, we could think that these are irreversible losses, which impact the $v(i)$_3 cycle. However, this statement should be tempered because MEA 4 comes from a different production batch. This could have an effect on its behaviour that makes the comparative analysis questionable.

Comparison of $v(i)$_1 and $v(i)$_3, performed in a different current direction, i.e. exploring the currents in an increasing manner and vice versa, confirms that this technology does not exhibit significant hysteresis. This can be seen in Fig. 7 where the first $v(i)$ of these two cycles are well superposed.

4.2 Proposal to improve the break-in process

The realization of EIS on the different steps of the $v(i)$ revealed an interest, to carry out $v(i)$ in cycling in order to extend the running-in procedure of the MEA manufacturer. Indeed, the EIS allows the access to the measurement of the high-frequency resistance R_{HF}, which is identified in the models with a R_{cell} resistance, attributed to the resistive phenomena taking place in the fuel cell [15]. It can be observed to decrease over time before stabilizing during the $v(i)$_1 and $v(i)$_2 cycles. This resistance is used in the quasi-static modeling of the HT-PEMFC, in a voltage loss term which is subtracted to the reversible voltage (see equation 2) [15].

$$\eta_{ohm}=R_{cell}\, j_{cell} \tag{2}$$

For the $v(i)$_1 cycle, the voltage gain provided by the R_{HF} decrease is then maximal at 1 A.cm^{-2} (+5 mV). It is a part of the gain that is also observed between the initial and the final reference $v(i)$ of the $v(i)$_1 cycle (+8 mV, cf. Table 2). Thus, a perspective is considered to extend the break-in period. The $v(i)$_1 cycle could therefore be performed, after the break-in period proposed by the manufacturer. It would improve performance and ensure good repeatability of the $v(i)$, by measuring the R_{HF}. This cycle would then stop at the moment of stabilization of this resistance and validation by the repeatability of the $v(i)$. This last $v(i)$ would then constitute the initial reference polarization curve of the test.

4.3 About degradation

The test campaign presented was also carried out on a similar test bench in order to check the reproducibility of the results. The different cycles were performed at the same time in order to be at the same atmospheric pressure. Moreover, this second test bench presented a CO_2 sensor at the cathode gas outlet. In order to protect the sensor from humidity, additional condensation and liquid purging equipments are also present. Due to current regulation problems, all results are unfortunately not usable. However, we note similarities in the results for the initial phases of the tests and for the voltage variations during the first half of the cycles.

If we look at the measurements of the CO_2 sensor, it seems that the degradation observed by S. Rigal et al is at least partly caused by carbon corrosion. Indeed, above a certain voltage, a CO_2 emission (attributed to the carbon corrosion reaction) has been observed. This emission seems to be more important, following the transition to the open circuit voltage (see Fig. 10). Note that the sensor

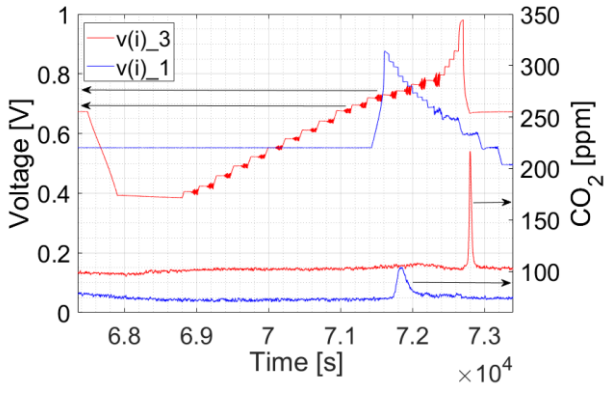

Fig. 10. Voltages recorded during two different $v(i)$ (from $v(i)\_1$ and $v(i)\_3$) and the corresponding CO_2 peaks).

is not located directly after the fuel cell cathode outlet. There is therefore a time lag between the CO_2 emission by the fuel cell and its reception by the sensor. Consequently, this time lag depends on the gas flow and the pipe volume. Thus, it explains why the cycle $v(i)\_3$ is not at the same global voltage gain level as $v(i)\_1$ and $v(i)\_4$.

5 Conclusion

The proposed cycling method is therefore validated in order to compare $v(i)$. However, the analysis will have to be prolonged with regard to the stabilities of the operating conditions and the modelling to be truly complete. Meanwhile, this investigation has helped to better understand in which way a $v(i)$ could be more or less degrading. The degradation linked to the passage to low current densities has been highlighted as being CO_2 emitting by the carbon corrosion mechanism. It seems to be intensified by the passage to the open-circuit voltage. Thus, the use of these MEA at OCV, even for short times during the realization of the $v(i)$, should be prohibited. Also, cycling of $v(i)$ could have a beneficial effect on the fuel cell. An extension of the break-in period could then consist in performing several polarization curves, until the R_{HF} parameter is stabilized and the $v(i)$ are superposed in repeatability. This could improve the reproducibility at the beginning of the MEA life, thanks to the monitoring of the R_{HF}. Finally, thanks to the observations and analyses, it will be possible to design a $v(i)$ methodology for future tests that is the less degrading as possible. This $v(i)$ can then be experimented on stack. It will also be interesting to analyze the other characterizations, by the experimental methodology proposed in this article.

The authors would like to express their sincere thanks to all the members of the PIPAA project, it is to say Safran Power Units, the LAPLACE laboratory and to the PBI (Banque Publique d'Investissement). The authors would like also to thank all the public funders (FEDER, Occitanie Region, French Government, and Toulouse Metropole) of the LAPLACE Hydrogen Platform used for all tests during the PIPAA project.

References

1. D. S. Lee, D. W. Fahey, A. Skowron, M. R. Allen, U. Burkhardt, Q. Chen, S. J. Doherty, S. Freeman, P. M. Forster, J. Fuglestvedt, A. Gettelman, R. R. De León, L. L. Lim, M. T. Lund, R. J. Millar, B. Owen, J. E. Penner, G. Pitari, M. J. Prather, R. Sausen, and L. J. Wilcox, Atmospheric Environment **244**, 117834 (2021)
2. S. Gössling and A. Humpe, Global Environmental Change **65**, 102194 (2020)
3. Airbus, Global Market Forecast (2019-2038), airbus.com (2019)
4. Boeing, Commercial Market Outlook (2021-2040), boeing.com (2021)
5. McKinsey & Company, Hydrogen-powered aviation, fch.europa.eu (2020)
6. Safran, Le projet collaboratif PIPAA, safran-group.com (2017)
7. DOE, Workshop on Fuel Cells in Aviation, energy.gov (2011)
8. J. R. Vang, F. Zhou, S. J. Andreasen, and S. K. Kaer, ECS Transactions **68**, 13 (2015)
9. A. Chandan, M. Hattenberger, A. El-kharouf, S. Du, A. Dhir, V. Self, B. G. Pollet, A. Ingram, and W. Bujalski, Journal of Power Sources **231**, 264 (2013)
10. T. J. Schmidt and J. Baurmeister, Journal of Power Sources **176**, 428 (2008)
11. T. J. Schmidt, in *Polymer Electrolyte Fuel Cell Durability*, edited by F. N. Büchi, M. Inaba, and T. J. Schmidt (Springer, New York, NY, 2009), pp. 199–221
12. S. Authayanun, K. Im-orb, and A. Arpornwichanop, Chinese Journal of Catalysis **36**, 473 (2015)
13. K. Scott, S. Pilditch, and M. Mamlouk, J Appl Electrochem **37**, 1245 (2007)
14. R. Sood, *Electrolytes polymère nano-structurés à base de liquides ioniques pour les piles à combustible hautes températures*, phdthesis, Université de Grenoble (2012)
15. S. Rigal, C. Turpin, A. Jaafar, N. Chadourne, T. Hordé, and J.-B. Jollys, in *2019 IEEE 12th International Symposium on Diagnostics for Electrical Machines, Power Electronics and Drives (SDEMPED)* (2019), pp. 439–445
16. S. Rigal, C. Turpin, A. Jaafar, T. Hordé, J.-B. Jollys, and N. Chadourne, Fuel Cells **20**, 272 (2020)
17. A. D. Modestov, M. R. Tarasevich, V. Ya. Filimonov, and N. M. Zagudaeva, Electrochimica Acta **54**, 7121 (2009)
18. Y. Oono, A. Sounai, and M. Hori, Journal of Power Sources **189**, 943 (2009)
19. Z. Qi and S. Buelte, Journal of Power Sources **161**, 1126 (2006)
20. S. Galbiati, A. Baricci, A. Casalegno, and R. Marchesi, International Journal of Hydrogen Energy **38**, 6469 (2013)
21. Q. Li, D. Aili, H. A. Hjuler, and J. O. Jensen, *High Temperature Polymer Electrolyte Membrane Fuel Cells: Approaches, Status, and Perspectives* (2016)